The Attribution of Land–Atmosphere Interactions on the Seasonal Predictability of Drought

JOSHUA K. ROUNDY* AND ERIC F. WOOD

Department of Civil and Environmental Engineering, Princeton University, Princeton, New Jersey

(Manuscript received 24 June 2014, in final form 18 October 2014)

ABSTRACT

Drought has significant social and economic impacts that could be reduced by preparations made possible through seasonal prediction. During the convective season, when the potential of extreme drought is the highest, the soil moisture can provide a means of improved predictability through land–atmosphere interactions. In the past decade, there has been a significant amount of work aimed at better understanding the predictability of land–atmosphere interactions. One such approach classifies the interactions between the land and the atmosphere into coupling states. The coupling states have been shown to be persistent and were used to demonstrate the existence of strong biases in the coupling of the NCEP Climate Forecast System, version 2 (CFSv2). In this work, the attribution of the coupling state on the seasonal prediction of precipitation and temperature and the extent to which the bias in the coupling state hinders the prediction of drought is analyzed. This analysis combines the predictions from statistical models with the predictions from CFSv2 as a means to isolate and attribute the predictability. The results indicate that the intermountain region is a hotspot for seasonal prediction because of local persistence of initial conditions. In addition, the local persistence of initial conditions provides some level of drought prediction; however, accounting for the spatial interactions provides a more complete prediction. Furthermore, the statistical models provide more skillful predictions of precipitation during drought than the CFSv2; however, the CFSv2 predictions are more skillful for daily maximum temperature during drought. The implication, limitations, and extensions of this work are also discussed.

1. Introduction

Drought has significant economic impacts that are estimated to have an annual average cost of $6–8 billion in the United States (Wilhite 2000). In recent years there have been two extreme droughts (2011 and 2012) that have affected a historically large fraction of the country, including the primary growing regions (Karl et al. 2012). The ability to predict such droughts would allow for preparations that could minimize the impact of these extreme events. The source of predictability of the atmosphere on a seasonal time scale lies in the slowly varying boundary conditions (i.e., sea surface temperatures and land surface characteristics) and can provide skillful seasonal forecasts to the extent that these boundary conditions are predictable (Palmer and Anderson 1994; Goddard et al. 2001). In particular, during the convective season, when the potential of extreme drought is the highest, the soil moisture can provide a means of improved predictability through land–atmosphere interactions (Koster et al. 2000).

There has been a great deal of work over the last decade to quantify land–atmosphere interactions and feedbacks over a variety of scales that utilize observations and prediction models. Working groups as part of the Global Energy and Water Cycle Experiment (GEWEX) initiative have done much of this work. One such effort focuses on the local land–atmosphere coupling through diagnosing the interactions between the land surface and the planetary boundary layer for models and observations using high-resolution test beds (Santanello et al. 2009, 2011). Other analyses have looked at the land–atmosphere interactions of models at the scale of GCMs (Dirmeyer et al. 2006), including the

* Current affiliation: Hydrological Sciences Branch, NASA Goddard Space Flight Center, Greenbelt, Maryland.

Corresponding author address: Joshua K. Roundy, Goddard Space Flight Center, Building 33, Room G209, Greenbelt, MD 20771.
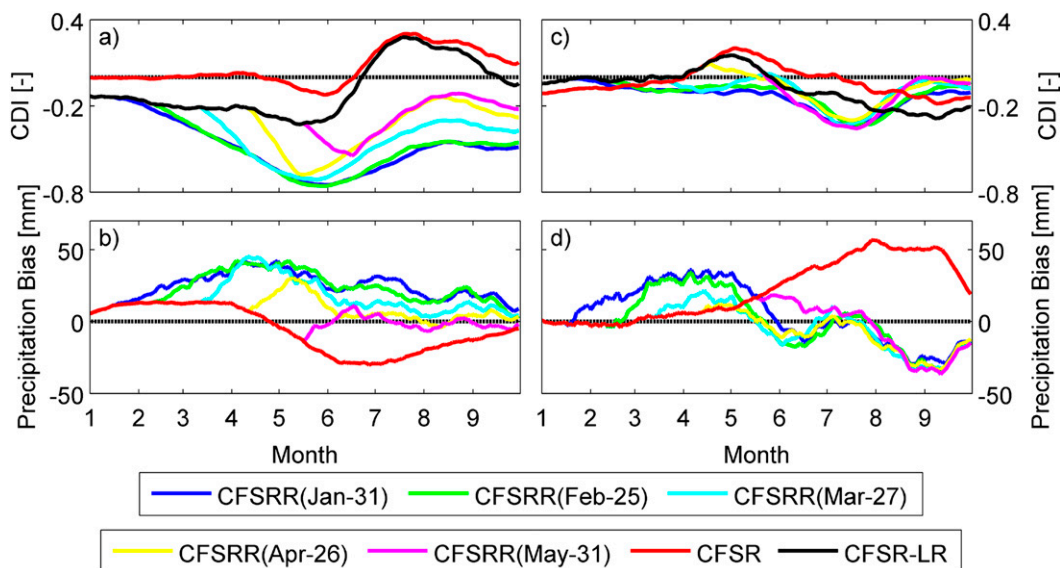E-mail: joshua.roundy@nasa.gov

FIG. 1. The 28-yr average of the 30-day (a),(c) CDI and (b),(d) cumulative precipitation bias relative to NLDAS-2 for CFSR, CFSR-LR, and forecasts conditioned at five different initialization times over the (left) Great Plains (33.75°–43.75°N, 103.75°–93.75°W) and (right) southeastern United States (25°–37.5°N, 91.25°–76.25°W). This is Fig. 3 from Roundy et al. (2014).

Global Land–Atmosphere Coupling Experiment (GLACE) phase one (Koster et al. 2006; Guo et al. 2006) and phase two (Koster et al. 2011). A promising addition to these studies is the use of satellite remote sensing to classify and understand land–atmosphere interactions at the GCM scale (Ferguson and Wood 2011; Taylor et al. 2012).

Recent work by Roundy et al. (2013) has added to the understanding of drought and land–atmosphere interactions by using reanalysis and remote sensing over the southeastern United States to classify each day into dry, wet, transition, or atmospherically controlled coupling regimes. The classification of the coupling state relies on two atmospheric measures, the convective triggering potential (CTP) and low-level humidity index (HI) following the approach of Findell and Eltahir (2003). The CTP is a measure of atmospheric stability and is calculated by integrating the region between the atmospheric profile and the moist adiabatic temperature lapse rate. The HI is a measure of atmospheric humidity and is defined by the 50–150 hPa above ground level dewpoint depression. The CTP–HI space is then divided into the four coupling regimes based on the localized statistics of surface soil moisture. The rationale for this approach is that there is an inherent connection between the soil moisture and heat flux partitioning that dictates the land–atmosphere feedback and the temporal persistence of these coupling regimes. The Roundy et al. (2013) classification of land–atmosphere coupling into four states—dry coupling, wet coupling, transitional, and atmospherically controlled (hereafter denoted as

"coupling state")—demonstrated a strong temporal persistence that was linked to precipitation characteristics for the dry coupling state (less-frequent and lower-magnitude precipitation) and wet coupling state (more-frequent and higher-magnitude precipitation). The temporal persistence and the net positive and negative feedback of the coupling state motivated the development of the coupling drought index (CDI). The CDI is a summary metric of the coupling state over a temporal period and is calculated by subtracting the number of dry coupling days by the number of wet coupling days, divided by the total number of days in the period and ranges from −1 (all wet coupling) to +1 (all dry coupling; Roundy et al. 2013).

The CDI was used by Roundy et al. (2014) to assess NCEP's Climate Forecast System, version 2 (CFSv2), by comparing the Climate Forecast System Reanalysis (CFSR) and Climate Forecast System Reanalysis and Reforecast (CFSRR). The comparison indicated that there was a long-term bias toward the wet coupling state in the CFSv2 forecasts (i.e., a more negative CDI), which correlates well with the precipitation bias. The quick deviation of the CFSRR forecasts from the CFSR and the low-resolution subset CFSR-LR (which is consistent with the vertical and horizontal resolution of the CFSRR dataset) into a wetter coupling state relative to the reanalysis is demonstrated in Fig. 3 from Roundy et al. (2014) and is included in this paper as Fig. 1. The tendency to a wet coupling state and a wet precipitation bias in the forecasts can be seen for both the Great

Plains (Figs. 1a,b) and the southeastern United States (Figs. 1c,d) but is more pronounced in the Great Plains. In addition, the results from Roundy et al. (2014) also showed that the wet coupling bias inhibits the representation of the extreme temperature and minimal rainfall during drought in the CFSv2 forecasts.

Although the work of Roundy et al. (2014) clearly indicates that the actual representation of drought events is severely limited in the CFSv2 model because of a bias in the coupling, the extent to which this bias limits the prediction of the year-to-year variability is unknown. Furthermore, the attribution of the coupling state to seasonal prediction of precipitation and temperature has yet to be explored. This work aims to bridge this gap in knowledge by analyzing the attribution of the coupling state on the seasonal predictability of precipitation and temperature in the CFSv2 model and its impact on drought prediction. To isolate the predictive nature of the coupling state, two statistical seasonal forecast models are developed. One of these statistical models relies only on the persistent nature of the initial coupling state to predict the future coupling state. The other statistical model aims to understand the impact of the bias in the coupling state by statistically correcting the bias in the coupling state from CFSv2. These two statistical prediction models of the coupling state are then combined with a statistical model of precipitation and temperature that is conditioned on the coupling state. The statistically based predictions are compared with the CFSv2 forecasts in order to attribute the importance of initial conditions and an unbiased prediction of coupling on the seasonal predictions of precipitation and temperature and its role in drought prediction.

The datasets and an overview of the methodology, along with a brief discussion of the models and setup, are discussed in section 2. Section 3 provides a detailed description of the statistical models developed in this study, while the results of the model comparison, the attribution, and the impact on drought prediction are presented in section 4 and are discussed in section 5. The attribution framework presented here relies on several models and datasets and their interaction. Therefore, there are a number of acronyms and terminologies that are crucial for comprehension. Although each of these terms is defined in the text, a centralized list is provided in Table A1 in the appendix as a reference for the reader.

2. Datasets and methods

a. Datasets

Because of the nature of this study, it relies heavily on observations of drought-relevant variables, such as precipitation, temperature, and other observations relating to land–atmosphere interactions. The observations of precipitation and temperature are taken from the North American Land Data Assimilation System, version 2 (NLDAS-2; Xia et al. 2012). The NLDAS-2 dataset incorporates gauge, radar, and reanalysis datasets to provide a gridded observation-based dataset over the continental United States. The NLDAS-2 dataset has a 0.125° spatial resolution and an hourly temporal resolution that was temporally upscaled to daily precipitation and daily maximum and minimum temperature. The metric used to define the coupling state requires observations from the land and the atmosphere that are taken from the CFSR. The CFSR provides data at a 6-hourly time step and assimilates conventional observations and satellite measurements of many atmospheric variables. The horizontal resolution of the model is T382 (0.313°) and includes the Noah model (Ek et al. 2003), which solves the water and energy balance at the surface. Because of the biases in the CFSR precipitation and the potential of drift in the land surface states, all land states of moisture and temperature are updated every 0000 UTC in the CFSR with an offline version of the land model forced by observed precipitation with all other forcing variables from the forecast model (Saha et al. 2010). Although the CFSR is model based, it assimilates observations and provides a best estimate of spatially continuous fields of soil moisture and atmospheric variables needed to define the coupling state.

The CFSRR dataset provides a 28-yr hindcast dataset from 1982 to 2009. During this reforecast period, 9-month seasonal hindcasts were made four times daily at 0000, 0600, 1200, and 1800 UTC every 5 days starting on 1 January of each year. In this study, we use only the initializations in May (1, 6, 11, 16, 21, 26, and 31), which results in a 28-member ensemble. Although the core CFSv2 model used to generate the hindcasts (CFSRR) was mostly consistent with the model used in the reanalysis (CFSR), there are some differences. For instance, only select pressure levels were archived and made available in the CFSRR dataset, although the vertical resolution of CFSR and CFSRR are consistent. In addition, the CFSRR horizontal resolution is T126 (0.9375°) compared to T382 (0.313°) in the CFSR (Saha et al. 2014). The lower spatial resolution and the fewer number of archived variables in the CFSRR dataset was the motivation for developing a consistent CFSR dataset (CFSR-LR) by Roundy et al. (2014). For the remainder of this study, the CFSR-LR will be used and referred to as simply CFSR in order facilitate an equal comparison between the CFSRR and the CFSR. For consistency, all datasets are upscaled using bin averaging to a 1.25°

spatial resolution over the contiguous United States (CONUS; 521 grids).

b. Methods

In this study, the coupling state is defined using the classification from Roundy et al. (2013). Although the Roundy et al. (2013) classification of coupling includes four states, the transitional state is combined with the atmospherically controlled state, as it generally had a low frequency for most grid cells in the domain and allows for a reduction of parameters in the statistical models. Furthermore, the CDI, which is the primary means of assessing the coupling state, is not affected by combining the transitional and atmospherically controlled states. The statistical models used in this study consist of two parts, the prediction of the coupling state and the prediction of precipitation and temperature based on the coupling state. The statistical model parameters are estimated using observations of the coupling state from CFSR and NLDAS-2 for precipitation and temperature variables from 1979 through 2009. The hindcast period for evaluating the predictions is from 1982 through 2009. It would be ideal to have two distinct periods for model fitting and forecast evaluation; however, this is not possible given the temporal limitations of the observational and hindcast datasets. Therefore, in order to avoid overfitting the model, all parameter estimation uses a cross-validation framework that consists of removing a single year from the dataset and estimating the parameters. This process is repeated for each year in the dataset and results in multiple estimates of the same parameter equal to the number of years in the dataset used to fit the model. The final model parameter is taken as the mean of all estimated parameters.

The parameters of each model are discussed in detail in section 3 but are uniquely estimated for each month in order to capture the underlining seasonality. The seasonality in the daily simulations of coupling state, precipitation, and temperature is ensured by linear interpolation. The validation period is June–August (JJA), which is a season typified by strong impacts of land–atmosphere coupling in North America. The CFSRR includes a 28-member ensemble, but since statistical generation is not computationally limited the statistical ensembles include 1120 members, which is 40 times larger than the CFSRR. The forecasts are evaluated for nine validation periods that all start on 1 June, but extend through day 3, 5, 10, 15, 30, 45 (15 July), 61 (31 July), 76 (15 August), and 92 (31 August). The skill for each of these validation periods is assessed through the bias and the Spearman rank correlation between the observations and the ensemble mean. One disadvantage of using the ensemble mean is that as the number of

ensemble members increases, the difference in the year-to-year predictions is very small. This will not affect the skill in terms of the correlation, but it can impact the magnitude of the bias and anomalies. To avoid this, the variability of the ensemble means is rescaled by the variability of all ensemble members across all years. This provides a more realistic year-to-year variation in the forecasts that is based on the variability of the model.

3. Models

To attribute the importance of the coupling state and its bias in CFSv2 on the seasonal predictions of precipitation and temperature requires the isolation of different aspects of predictability. This is done through the coupling stochastic model (CSM), the coupling correction model (CCM), and the stochastic weather model (SWM). The details of the CSM, CCM, and the SWM, which are unique to this study, are discussed below, followed by a description of how these models are used to attribute the seasonal predictability.

a. Coupling stochastic model

The CSM is based on a conditional Markov chain process, that is, the future coupling state is dependent on the previous coupling state and the presence of precipitation. This results in two 3 × 3 matrices of transitional probabilities, one for precipitation greater than zero and one for no precipitation for each grid cell. Although each transitional matrix contains nine probabilities, only six of the probabilities need to be estimated, as the sum of the conditional probabilities has to equal one. Furthermore, in order to capture the seasonality of the coupling, it is necessary to estimate these transitional probabilities for individual months during the 5-month period from May to September. This gives a total of 12 estimated parameters per month for a total of 60 estimated parameters for each grid cell for the CSM. These probabilities are estimated from the CFSR observed coupling state and the NLDAS precipitation using the cross-validation framework (see section 2b) over the 28-yr hindcast period.

An example of the CSM is given in Fig. 2 for a grid in western Oklahoma. Of all the transitional probabilities, the persistent probabilities are the highest for each coupling state. Furthermore, these persistent probabilities are lower (higher) for days that were preceded by precipitation for a dry (wet) coupling state, respectively. However, the persistence of the atmospherically controlled state does not vary for days that were preceded by precipitation. This is consistent with the nature of coupling state defined by Roundy et al. (2013) in that the atmospheric regime is unaffected by the local conditions.
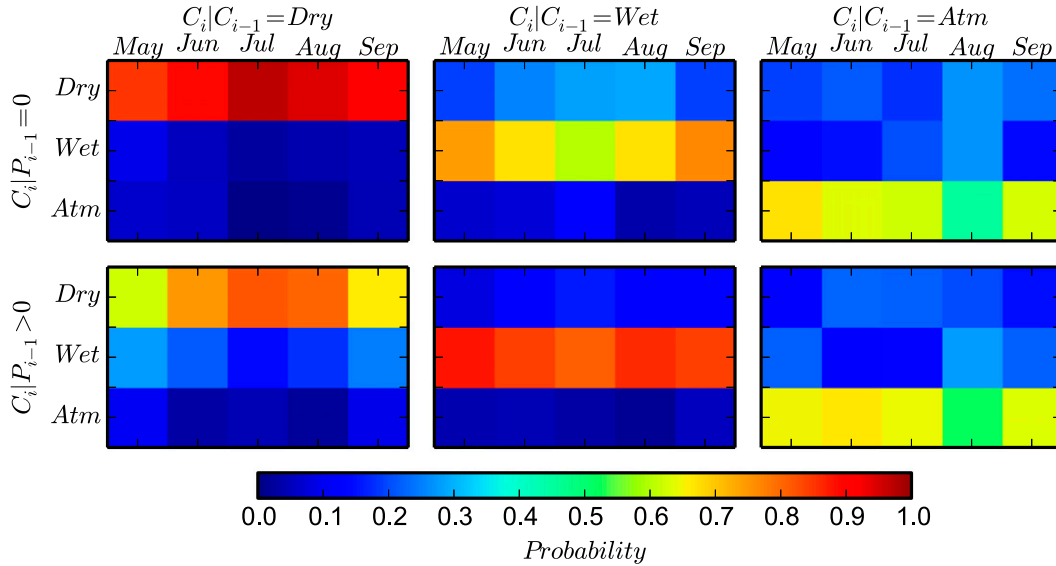
FIG. 2. The transitional probabilities conditioned on the previous day coupling state C_{i-1} and precipitation P_{i-1} that make up the CSM for an example grid in western Oklahoma (36.88°N, 100.62°W).

The predictability of the CSM relies on the persistence of the local initial conditions; however, the CSM uses both the initial state of coupling and precipitation. Therefore, in order to isolate the individual impact on predictability, two versions of the model are used. One initialization is based on randomly initializing based on the climatology of coupling state in May (CSMc) and the other is initialized by the observed May coupling state, weighted toward the latter half of the month, from CFSR (CSMr). Both versions of the model are initialized with the observed precipitation. These two initializations allow for an assessment of the relative importance of the initialization of the coupling state and precipitation.

b. Coupling correction model

The CCM is based on correcting the biases in the CTP and HI from CFSRR and reclassifying coupling in order to provide an unbiased prediction. The correction of the CTP and HI uses standard normal deviates (Koster et al. 2009) based on matching the mean and standard deviation of CFSRR (forecasts) to that of CFSR (observations) and is done seasonally from May to September. This gives a total of 20 estimated parameters (four per month) for the CCM. To avoid overfitting the correction model, the forecast mean and standard deviation are estimated from the 1800 UTC 26 April ensemble member and the cross-validation framework was used to estimate the mean and standard deviation of both the CFSRR and CFSR. Although the predictions of coupling state from CCM are merely a correction to the predictions made from CFSRR, it is still considered as a separate model because the corrected coupling state

can be used to generate unique and independent predictions of precipitation and temperature.

c. Stochastic weather model

The SWM predicts the precipitation, daily maximum temperature, and the daily minimum temperature based on the coupling state. The rationale for this relationship comes from the work of Roundy et al. (2013, 2014), which showed distinct differences in the precipitation and temperature statistics based on coupling state. In addition to coupling state, the probability of precipitation is also dependent on the previous day's precipitation, which is typical in point process precipitation models (Katz 1977). The SWM therefore consists of the probability of precipitation and the distributions of precipitation magnitude, maximum daily temperature, and minimum daily temperature for each coupling regime and month. The probabilities and distributions are estimated using observations from 1979 through 2009 and consist of 30 parameters for the probability of precipitation and 90 parameters for the distributions for a total of 120 parameters per grid cell for all months and coupling regimes. The distributions are fit using least squares optimization to a Weibull, Gamma, or Normal distribution. The distribution is chosen based on the p value from the Kolmogorov–Smirnov (KS) test using the full observational record; however, once the best distribution is chosen, the actual parameters are estimated using the cross-validation methodology. If a given sample had less than 30 observations, the monthly climatology was used. This occurred less than 5% of the time and was due to low frequencies of a particular coupling state. The precipitation distribution is fit to events above the 0.254-mm
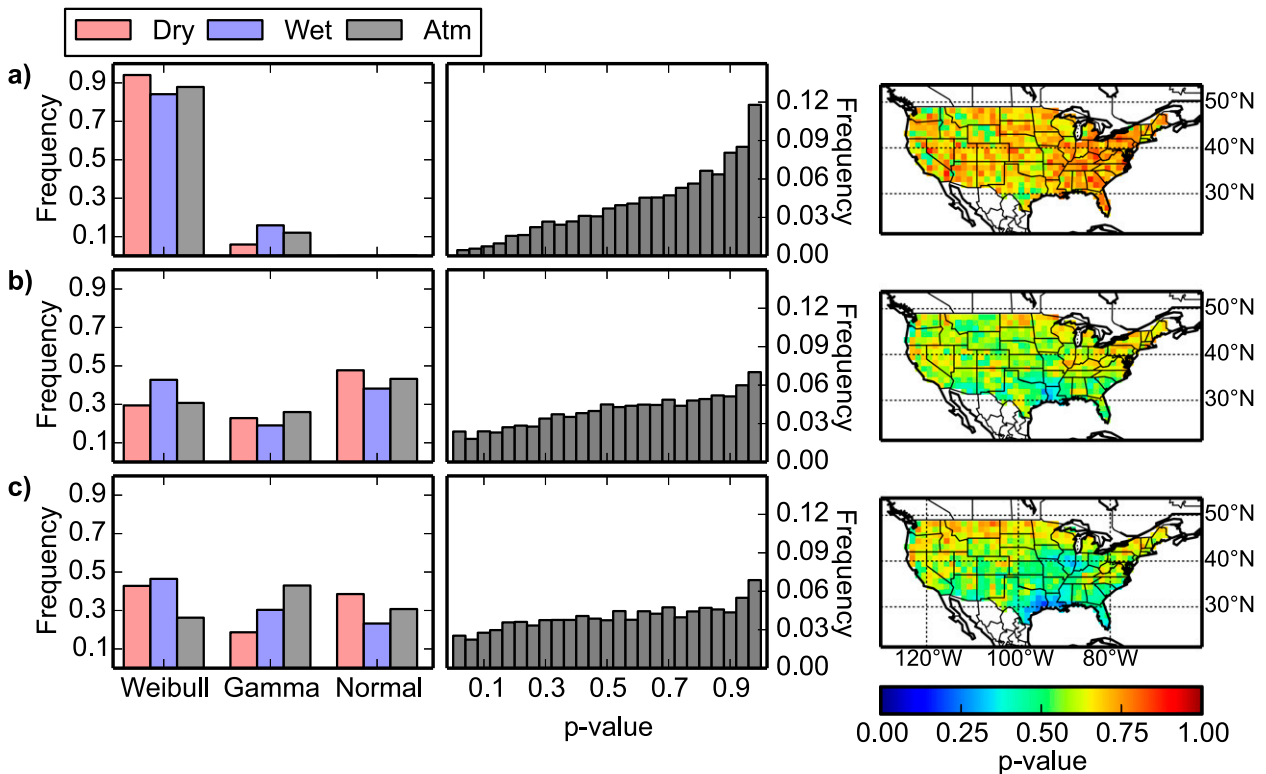
FIG. 3. The distribution frequency, the KS test p value for each fitted distribution (histogram), and the average p value at each grid for (a) precipitation, (b) daily max temperature, and (c) daily min temperature that are part of the SWM.

threshold and the temperature variables are fit using kelvins to ensure values above zero; however, the results will be displayed in degrees Celsius. Furthermore, to ensure that the daily maximum temperature is always larger than daily minimum temperature, the observed correlation between the two variables is conserved.

A summary of the fitted distributions and the goodness of fit are given in Fig. 3 and indicate that the most frequent distribution for precipitation was the Weibull, while for the daily maximum and minimum temperature it was the Normal distribution. For precipitation, almost 90% of distributions were Weibull, but the temperature variables are more equally spread out across all three distributions. The goodness of fit is assessed through the p value of the KS test, which is the probability of getting a similar KS statistic if the samples were randomly drawn from the same distribution. Therefore, the higher the p value, the better the fit. The histogram of p values indicates the precipitation had a better fit than the temperature variables. In particular, the eastern portion of the United States had the highest p values for precipitation, while the temperature fits were better in the northwest.

The SWM for a grid in western Oklahoma is given in Fig. 4, including the probability of precipitation and select percentiles from the distributions. The coupling state dependence on the probability of precipitation is indicated by the lowest probabilities for dry coupling and the highest for wet coupling for all seasons. This is further distinguished by the presence of precipitation on the previous day. In comparison, the atmospherically controlled state has more-frequent precipitation than the dry coupling and less frequent than the wet coupling state for most seasons. In addition, the atmospheric state also shows the most variability across the seasons. The percentiles from the precipitation distributions show a similar dependence on coupling state as dry coupling is the driest and the wet coupling is the wettest. The temperature distributions also show distinct differences between dry and wet coupling, with the dry coupling being warmer for both daily maximum temperature and daily minimum temperature; however, the difference is less intense for daily minimum temperature. In addition, there is also little difference between the wet coupling and atmospherically controlled distributions of temperature.

d. Modeling setup

The modeling setup used in this study is outlined in Fig. 5, which gives an overview of all the models and their connection with each other. The first thing
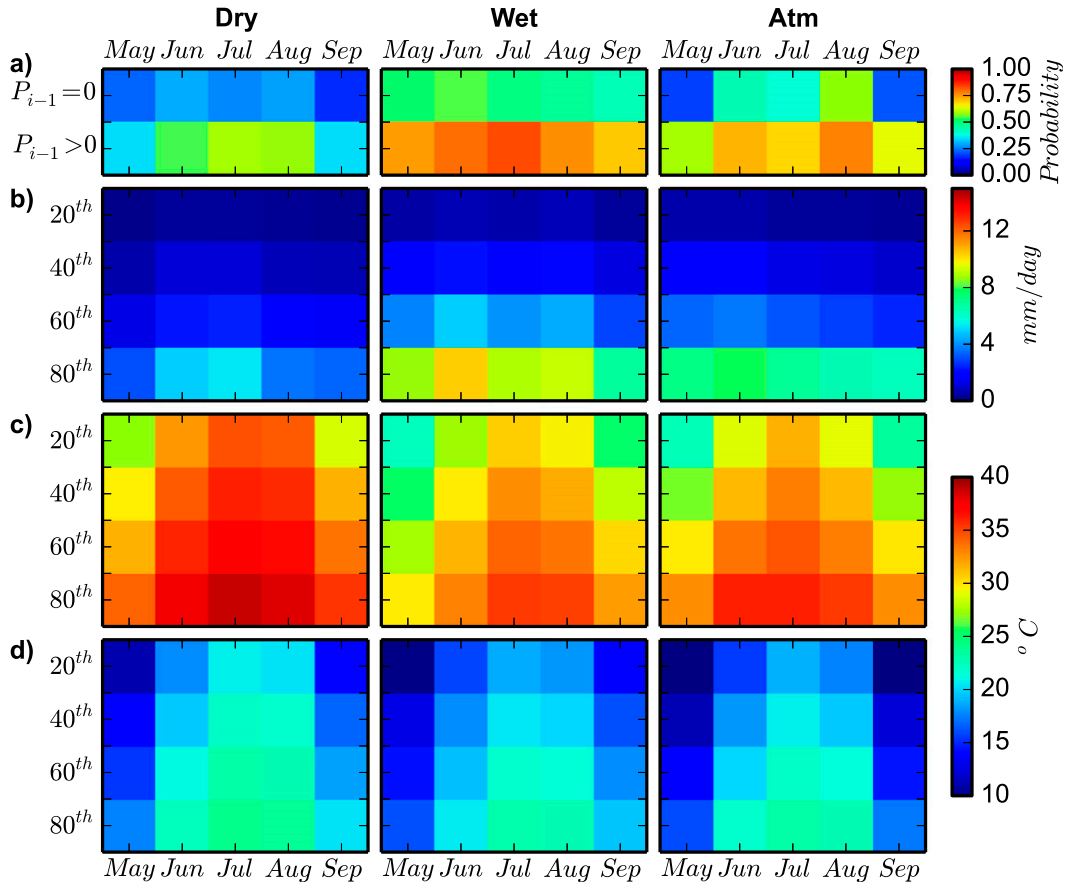
FIG. 4. The (a) probability of precipitation and (b)–(d) select percentiles from the distributions of precipitation intensity and daily max and min temperature dependent on coupling and season in the SWM for a grid in western Oklahoma (36.88°N, 100.62°W).

needed for all the prediction models is the initial conditions. For this study, only model predictions that are based on May initial conditions are used. The CFSR provides all the needed boundary conditions for running the CFSRR (gray) forecasts. In comparison, the CSM only requires the initial conditions of precipitation (from NLDAS-2) and the coupling state. The initial conditions of coupling state come from the observed CFSR coupling state (CSMr; blue) and the climatological coupling state from CFSR (CSMc; yellow). In addition to the two initializations of the CSM, the CFSRR dataset provides predictions of the coupling state. As discussed earlier, there are significant biases in these predictions of the coupling state from the CFSv2 model. Therefore, the CCM (green) is used to correct the known bias in the CFSRR coupling state.

In addition to the coupling prediction, the models also produce predictions of precipitation and daily maximum and minimum temperature. The CFSRR forecasts include predictions of these variables due to the fully coupled nature of the model; however, the statistical models only provide predictions of coupling. Therefore, the SWM is used to provide predictions of precipitation and temperature given the prediction of coupling from the CCM, CSMr, and CSMc. To assess the potential predictability of the SWM, the observed coupling from the CFSR is also treated as a forecast and is called the coupling potential model (CPM; red).

This setup provides a means to attribute and isolate the influence of the coupling state on the seasonal predictability of precipitation and temperature. For example, the predictions of precipitation and temperature from the CSMc are based solely on the observed initial conditions of precipitation. When analyzed with the CSMr, which uses observed initial conditions of precipitation and coupling state, it allows for the isolation of the predictability associated with observed initial coupling state. The predictions of precipitation and temperature from the CCM provide a hybrid approach that combines a bias-corrected dynamical prediction of coupling with a statistical simulation.
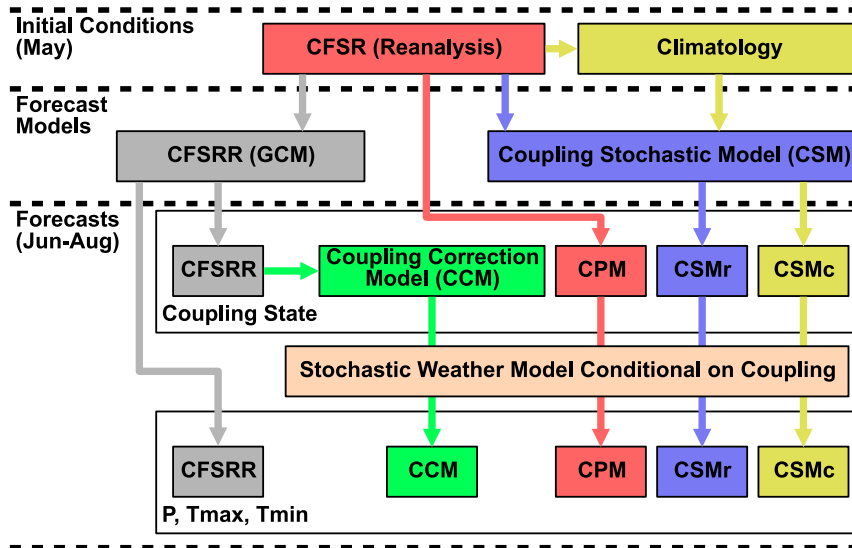
FIG. 5. A diagram of the initial conditions, models, and forecasts used in this study and their interactions.

When analyzed with the CFSRR, this allows for an isolation of the predictability of precipitation and temperature associated with a fully coupled prediction of the coupling state that is not affected by the bias of the coupling state. Furthermore, the predictions of the precipitation and temperature from the CPM provide a means to understand the upper limit of predictability associated with predictions based on the coupling state. Comparing all of these predictions provides a means to attribute the impact of the coupling state on the overall predictability and the prediction of drought.

4. Results

a. Model comparison and predictability

As indicated by Fig. 1, one of the main limitations of the precipitation and temperature forecasts from CFSv2 are the strong biases in their predictions. As such Fig. 6 gives the bias in the forecasts of coupling state, precipitation, and temperature during the 28-yr hindcast period for the JJA validation period for the CFSRR, CCM, and CSMr. The CFSRR shows strong biases across all variables (Fig. 6a). In particular, the CDI
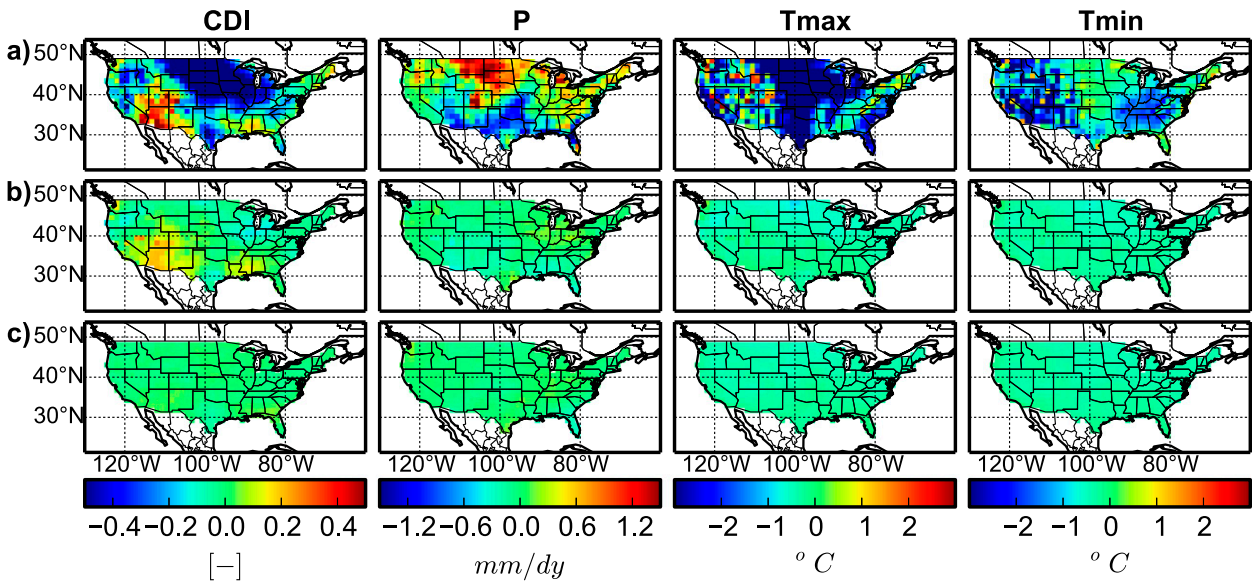

FIG. 6. The 3-month (JJA) validation period bias for the CDI, precipitation P, daily max temperature Tmax, and daily min temperature Tmin for (a) CFSRR, (b) CCM, and (c) CSMr.
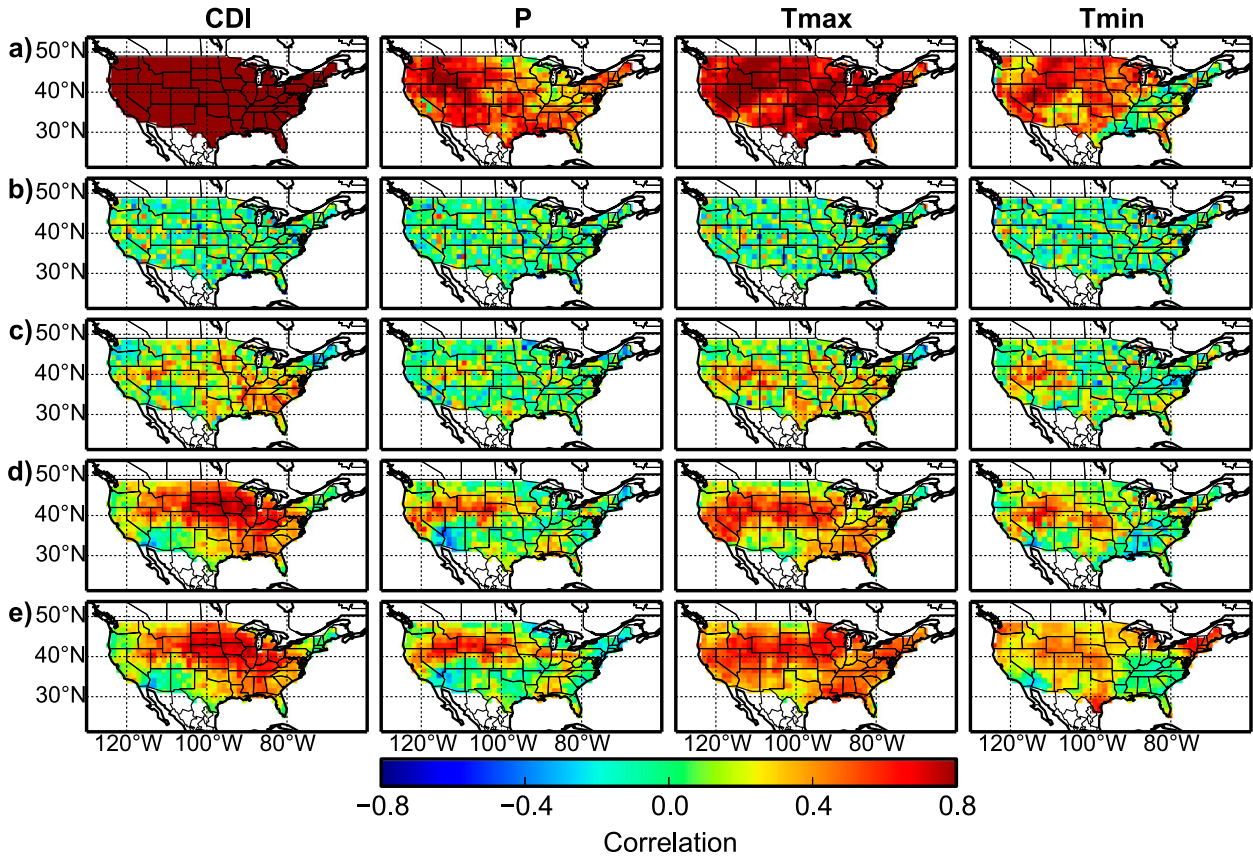
FIG. 7. The 3-month (JJA) validation period skill (Spearman correlation) for CDI, *P*, Tmax, and Tmin for (a) CPM, (b) CSMc, (c) CSMr, (d) CCM, and (e) CFSRR.

shows a strong negative bias over most of the country, with the exception of the Southwest and portions of Mississippi and Alabama, which have a positive bias. In comparison, the precipitation shows a strong positive bias in the north and a negative bias in the south. Although there is some connection between the bias in the CDI and the precipitation (north-central and Southwest), the precipitation bias is not completely described by the CDI. On the other hand, the daily maximum temperature shows a very strong negative bias that is reasonably correlated with the negative bias of the CDI. In contrast, the daily minimum temperature has the lowest bias in the areas where the daily maximum temperature bias is the highest. The CCM (Fig. 6b), which corrects the coupling state bias from the CFSRR and statistically generates precipitation and temperature, still has a small positive bias for the CDI in the southwest and southeast, but shows a large improvement in the bias compared to CFSRR. This indicates that the correction model is effective at removing the bias in the coupling. Furthermore, the forecasts of precipitation and daily maximum and minimum temperature show

little or no bias and offer a dramatic improvement over the CFSRR forecasts. The CSMr (Fig. 6c), which statistically simulates the coupling, precipitation, and temperature, has virtually no bias in any of the variables. Likewise, the CSMc and CPM (not shown) also have little or no bias in any of the variables. Although Fig. 6 does not account for the statistical significance of the bias, it demonstrates the differences between the models.

Although it is important for a prediction to be unbiased, it does not ensure the skill of the prediction. For instance, using the mean as a prediction for each year would also be unbiased, but would have no predictability. The predictability (Spearman correlation) over the 28-yr hindcast period is shown in Fig. 7 for the JJA validation period for CDI, precipitation, and daily maximum and minimum temperature for all the models. The CPM (Fig. 7a) shows a perfect correlation for CDI because its predictions of coupling state are the observations. Although the CPM prediction of coupling state is not useful, using a perfect prediction of coupling state provides a tool for assessing the potential predictability

of precipitation and temperature. The CPM indicates that the potential predictability of precipitation is the strongest in the Idaho area and the weakest in the Great Lakes. In comparison, the daily maximum temperature has a stronger potential predictability that covers the entire United States. In contrast, the daily minimum temperature shows the lowest potential predictability with a large portion from the Southeast to the Northeast with no predictability.

The predictability of the CSMc, which is a purely statistical model initialized with climatological initial conditions of coupling, is given in Fig. 7b and indicates that there is no spatial consistency in the predictability for coupling state, precipitation, or temperature. In comparison, the CSMr (Fig. 7c) uses observed initial conditions of coupling state and has skill for the CDI predictions in the intermountain region, parts of the Midwest and the Southeast, although there is still a considerable amount of noise. The transfer of coupling state predictability to precipitation is fairly weak, with only minor predictability in the intermountain region and parts of Texas. The temperature variables are more consistent with the CDI predictability, except over the Southeast for the daily minimum temperature where the potential predictability was low. The spatial noise in the CSMr predictability is likely due to the inherent randomness of the statistical generation and a lack of interaction and consistency among grid cells. Although the predictability of the CSMr is noisy, it clearly demonstrates superior predictability over the CSMc. This establishes the importance of the initial coupling state on seasonal predictability. The CCM, which corrects the bias in the coupling from the CFSRR and statistically generates predictions of precipitation and temperature (Fig. 7d), has a much stronger predictability of CDI, precipitation, and temperature and covers a greater spatial extent compared to the CSMr; however, there is still spatial consistency between the CSMr and CCM. This indicates that there is an enhancement of the predictability due to initial conditions by modeling the grid-to-grid interactions in a fully coupled land–atmosphere–ocean model. In addition, the predictability of the CFSRR (Fig. 7e) is nearly consistent with the CCM, but shows an increase in the predictability of precipitation and temperature. The difference in the predictability is particularly large for the daily minimum and maximum temperature. Although the CFSRR predictability is greater, the CCM still maintains most of the predictability and has the advantage of being unbiased.

To this point, only a 3-month (JJA) validation period has been considered and the change in predictability and bias for different validation lengths has not been established. The CONUS average bias and correlation for the nine validation periods is given in Fig. 8 for each of the five models. The bias in CDI of the models (Fig. 8a; CPM excluded) shows that the CFSRR bias is the highest and tends to increase as the length of the validation period increases, particularly for validations greater than 15 days. The strong biases seen in the CFSRR have been shown in several other studies (Roundy et al. 2014; Dirmeyer 2013). The other models show a much smaller bias that tends to decrease with time. The CDI correlation (Fig. 8e) for CFSRR and the CCM are nearly equal and show relatively little change in skill for validation periods less than 15 days after which the skill begins to decrease. In comparison, CSMr shows less skill, which begins to decrease immediately, and the absence of observed initial conditions in the CSMc leads to no seasonal skill, as shown previously. The precipitation bias (Fig. 8b) for all the models tends to decrease as the validation period increases; however, the CFSRR is much higher than the other models. The precipitation correlation (Fig. 8f) for the CSMc has no skill; the CFSRR, CCM, and CSMr show initial skill that decreases with time; and the CPM shows skill that increases as the validation period increases before reaching an asymptote. The bias of the daily maximum and minimum temperature (Figs. 8c,d) is relatively stable or decreases with time but then increases. However, the CFSRR has a larger bias that increases sooner and at a faster rate than the statistical models. The correlation of the daily maximum and minimum temperature (Figs. 8g,h) is similar to precipitation in that the CSMc has no skill; the CSMr, CCM, and CFSRR decrease; and the CPM increases with validation period. The increase in skill with validation period of the CPM is due to the perfect forecast of coupling state and the statistical generation of precipitation and temperature. Because the precipitation and temperature are statistically generated, it is unable to get the exact timing of the events, but as the validation period increases the importance of timing decreases. This leads to the skill of the CPM to increase to the level of predictability at which the coupling state explains the variability of precipitation and temperature. This asymptote indicates the upper limit of predictability of precipitation due to the variability of coupling state.

Although there are several interesting aspects of Fig. 8, one of the most useful is the attribution of predictability in the CFSv2 modeling framework that can be assessed by considering the difference in predictability between the models. For example, the area between zero and the CSMr in Figs. 8f–h is the portion of predictability due to the persistence of the local coupling state, as the only mode of predictability in the CSMr is the local initial conditions. In comparison, the area
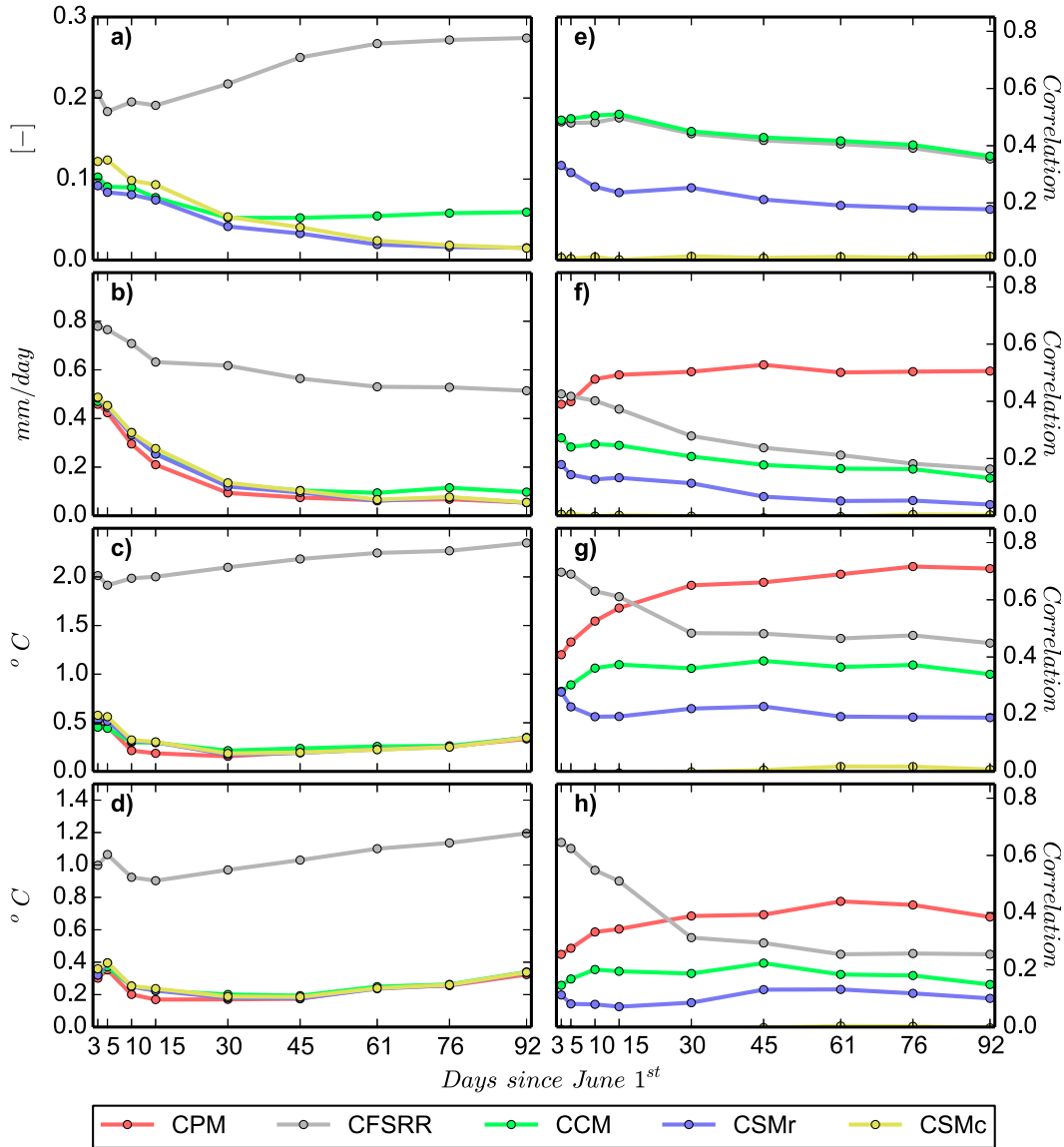
FIG. 8. The CONUS average model (a)–(d) bias and (e)–(h) Spearman correlation with validation period starting 1 Jun for CDI, *P*, Tmax, and Tmin, respectively.

between the CSMr and CCM is the attribution of predictability due to a dynamic prediction of coupling state that accounts for the interaction between grid cells. Similarly, the area between the CCM and the CFSRR represents the attribution of predictability from the dynamical model not associated with the coupling state (noncoupling). All these areas can be represented numerically by a fraction of the total predictability (area from 0 to 1) in order to understand the spatial extent and attribution of seasonal forecast predictability.

One difficulty in calculating these attributions is due to the inherent randomness in the predictability of the CSMr (Fig. 7c), which can cause random variability in

the attribution. This noise in the prediction is reduced by spatially averaging the grid cells within a two-grid radius of the center grid, for example, a 5 × 5. An example of the calculation of the attribution metric for a grid cell in western Oklahoma for daily maximum temperature is given in Fig. 9a. For this grid cell, the local coupling predictability fraction makes up 0.32 as indicated by the area between the CSMr and zero. Likewise, the dynamic coupling predictability fraction is made up of the area between the CSMr and CCM and is 0.08. The noncoupling predictability fraction is 0.1 from the area between CCM and CFSRR. This indicates that for this grid cell the local coupling or the persistence of the
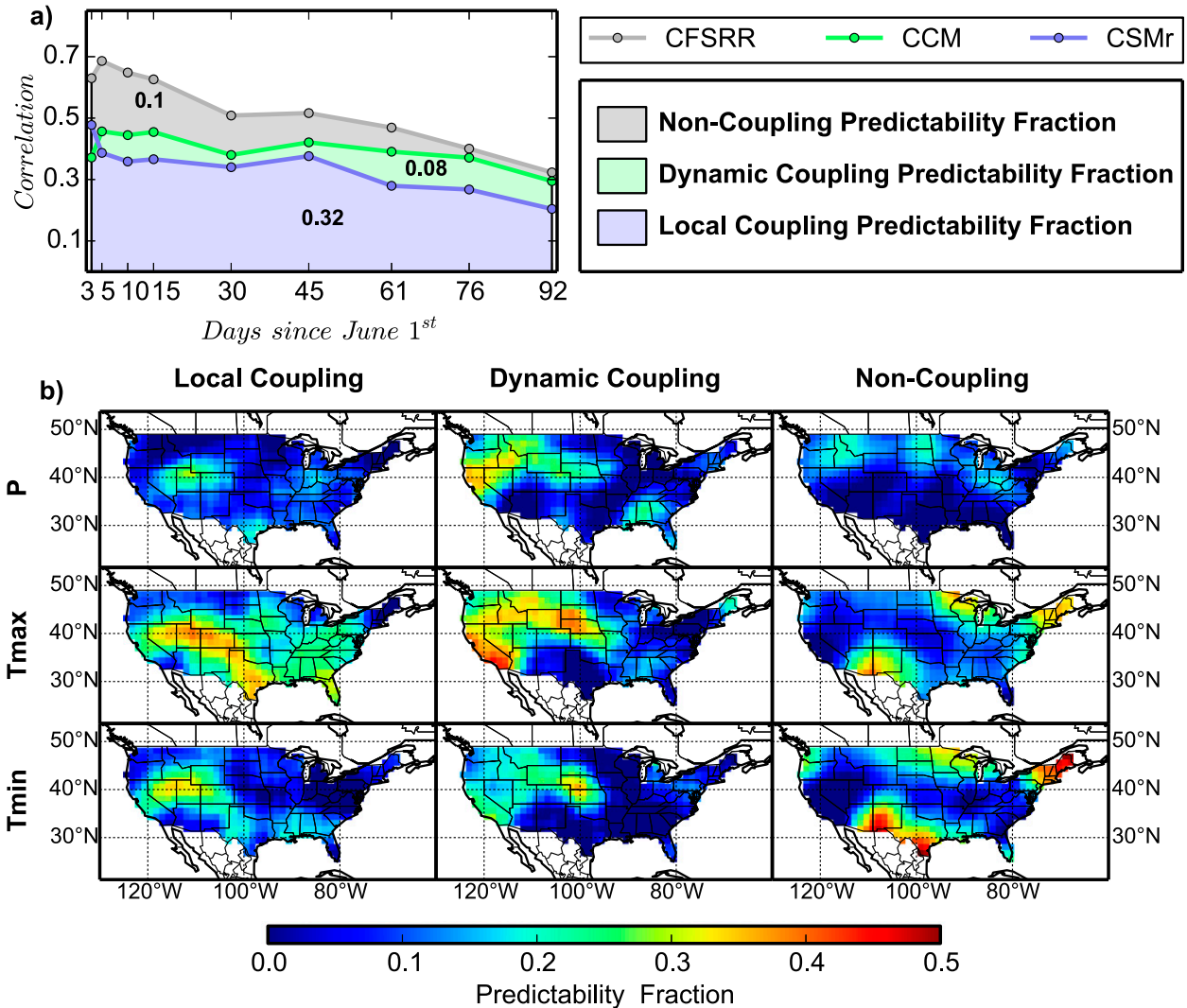
FIG. 9. (a) The fraction of predictability for Tmax due to local coupling, dynamic coupling, and noncoupling demonstrated for a single grid in western Oklahoma (36.88°N, 100.62°W) and (b) the spatial variability of the predictability fractions for P, Tmax, and Tmin.

initial conditions makes up the largest portion of the predictability.

The spatial variability of the different predictability fractions is given in Fig. 9b and indicates that the attribution of local coupling on seasonal prediction is the strongest for daily maximum temperature, followed by daily minimum temperature and precipitation. For precipitation the local persistence of initial conditions contributes about 20%–30% of the predictability, but only for a portion of the intermountain region. The local coupling predictability of daily maximum temperature has a much greater spatial extent with a contribution of over 40% for parts of the intermountain region and extends to parts of the Midwest and eastern United States at a smaller fraction of predictability. The local coupling predictability of daily minimum temperature is also the

strongest in the intermountain region, but does not cover the extent or magnitude of the daily maximum temperature. The attribution of predictability due to a dynamic prediction of coupling is mostly isolated to the west of the Mississippi River, except for a small area in the Southeast. Again, the attribution for the daily maximum temperature both in terms of extent and magnitude is greater, but all three variables show a similar area from the West Coast through the northern Great Plains. The attribution due to noncoupling has the smallest spatial extent of the three attributions, although it does have a particularly strong magnitude for the daily maximum and minimum temperature for the Southwest and Northeast. There is also a significant fraction of the predictability that is simply not predictable for some grids, that is, the sum of local coupling, dynamical coupling, and noncoupling is
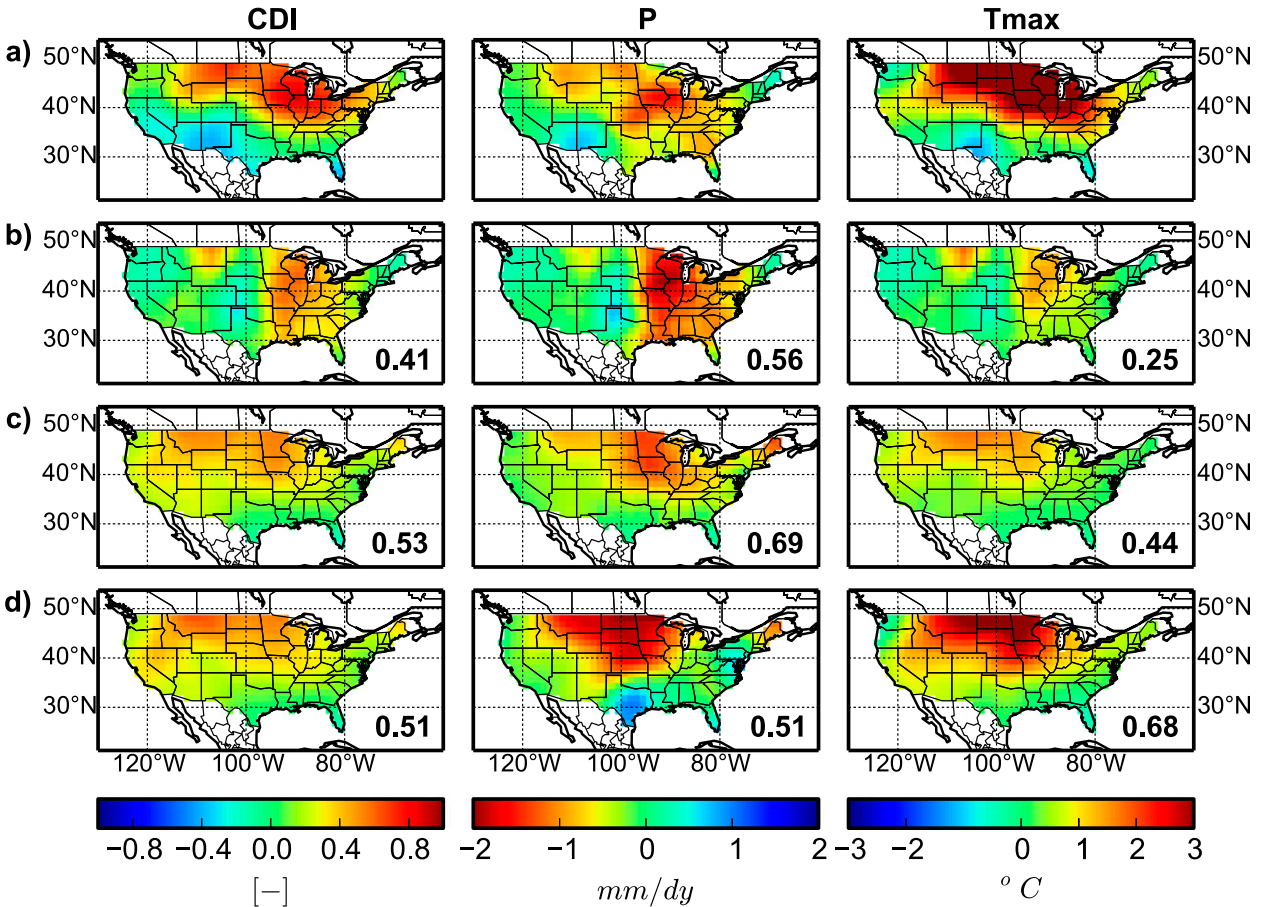
FIG. 10. The 1988 drought given by the JJA validation period anomalies of (a) observations and forecasts from (b) CSMr, (c) CCM, and (d) CFSRR with the TS for spatial drought prediction given in the lower-right corner for CDI, *P*, and Tmax.

not 1.0. Although the unpredictable fraction is not shown, it can be seen that, particularly for precipitation in the eastern part of the United States, the fraction of predictability that is attributed as unpredictable is large.

b. Predictability of drought

To this point, only the overall predictability of the models has been considered; however, the predictions of extremes, such as drought, are often the most crucial. The predictability of drought during the JJA validation period from the May initial conditions is analyzed over the hindcast period for each year by using the anomalies. Using anomalies provides a fair comparison across models for a single event without a consistent bias (i.e., CFSRR; Fig. 6a) influencing the results. The forecast anomalies are calculated from the rescaled ensemble mean and were spatially averaged, along with the observation anomalies, using a two-grid radius surrounding each grid cell. The spatial averaging was done to smooth out the inherent noise in the CSMr. The anomalies of the CDI, precipitation, and daily maximum

temperature for the observations, CSMr, CCM, and CFSRR are given in Fig. 10 for the JJA validation period in 1988. The observations (Fig. 10a) show a strong drought in the anomalies of the CDI, precipitation, and temperature in the northern part of the United States. Generally, there is a good match of the drought area among the variables; however, the CDI and the daily maximum temperature are the most consistent. The forecast anomalies from the CSMr (Fig. 10b) are somewhat consistent with the observations in terms of drought area. Numerically, this is assessed by calculating the spatial threat score (TS), which is the number of hits (forecast drought and observed drought) divided by the sum of the hits, false alarms (forecast drought and observed no drought), and misses (forecast no drought and observed drought). The TS is calculated spatially based on the number of grid cells that are observed and forecasted in drought. Drought is defined based on a threshold anomaly of 0.3, $-0.5 \, \mathrm{mm \, day^{-1}}$, and 1°C for the CDI, precipitation, and daily maximum temperature, respectively. The TS provides a balanced summary
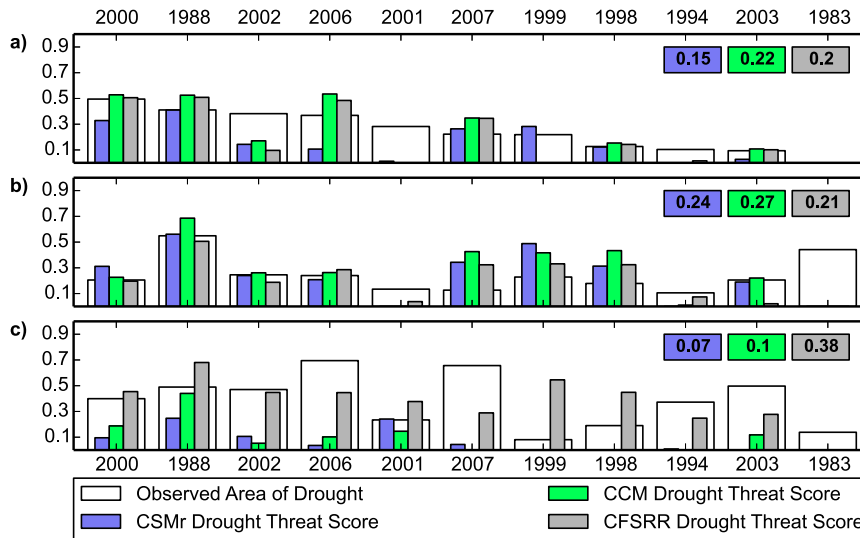
FIG. 11. The observed fraction of drought area over the CONUS based on anomaly thresholds and the spatial TS for drought prediction from the CSMr, CCM, and CFSRR for 11 drought years with the average TS given in the right corner for (a) CDI, (b) *P*, and (c) Tmax.

metric that considers correct spatial forecasts of drought (hits) while penalizing for poor spatial forecasts (false alarms and misses) that ranges from 0 (no skill) to 1 (perfect forecast) and is given in the lower-right corner of the plot. The TS for the CSMr (Fig. 10b) is the highest for the precipitation and the lowest for the daily maximum temperature. The CSMr fails to predict any drought in the Midwest (from Nebraska through the Dakotas) based on any of the variables, although it gets the drought on either side. This indicates that the persistence of initial conditions drove the drought on either side, but since the CSMr has no interaction between grid cells, the two droughts never connected. The CCM (Fig. 10c), which does account for grid-to-grid interactions in the coupling state, has a better agreement with the observations and predicts drought in the Midwest. This is indicated by a higher TS for the CCM compared to the CSMr for all variables. This illustrates the importance of grid-to-grid interactions to fully capture drought. In comparison to the CFSRR (Fig. 10d), the CCM has a slightly better TS for CDI (Fig. 10c); however, visually there is little difference. In contrast, there is a noticeable difference in the precipitation forecast, as the CFSRR does worse than both the CCM and the CSMr, but the CFSRR does better than both the CCM and CSMr for the daily maximum temperature.

Overall, there was fairly good predictability for the 1988 drought for all the models; however, each drought is different in terms of its mechanism and dynamics, and the predictability of the models is likely to vary for other drought years. Although a thorough evaluation of each drought in the hindcast period is not presented, using the

TS as a summary measure of drought predictability can still provide valuable insights. The TS for coupling, precipitation, and daily maximum temperature are shown in Fig. 11 for 11 drought years that had a fraction of drought area greater than 10% for two of the three variables (CDI, precipitation, and daily maximum temperature) and are ordered by the fraction of drought from the CDI. The first thing that is noticed is that there is a large variability in the drought prediction across drought years. For all variables, the 1988 drought is one of the strongest drought years and one of the most predictable by the models. In contrast, there are other years, such as 1983, when the models have no predictability of drought for any of the variables. The 1983 drought is also interesting, as the CDI does not indicate drought but the precipitation and temperature anomalies do. In comparison, in 2001 all variables indicate drought, but there is little or no predictability of coupling state and precipitation, and there is some predictability for daily maximum temperature. In general, as the area of CDI drought goes down, the predictability across all variables and models goes down, even though there is a fair amount of variability across drought events. Although there is considerable variability across drought events, the average TS across all drought years (given in the top-right corner of Figs. 11a–c) indicates that the CCM has the highest TS for coupling state, followed by the CFSRR and the CSMr. For precipitation, the CSMr and the CCM have a higher average TS than the CFSRR (Fig. 11b), and there are only a few drought years where the CFSRR does better (2006, 2001, and 1994). In 2006, the TS is only slightly higher for the

CFSRR as compared to years like 1988, 2007, 1999, and 1998, when the CCM does much better than the CFSRR for predictions of precipitation in drought years. Furthermore, in 2001 and 1994, the predictability of CFSRR for precipitation is very low. In contrast, CFSRR does much better than the CSMr and the CCM for the prediction of daily maximum temperature during drought.

5. Discussion and conclusions

In this study, statistical forecast models based on the coupling state were used to analyze and compare with seasonal forecasts from the CFSv2. The coupling stochastic model (CSM) provides forecasts of coupling state through a Markov chain model based on the persistence of the initial conditions. A second forecast model of coupling state was developed that corrected the bias in the coupling state from the CFSv2 forecasts and is named the coupling correction model (CCM). These statistically based predictions of coupling were then used to generate forecasts of precipitation and temperature using the stochastic weather model (SWM) that is conditioned on the coupling state. The predictions from the stochastic models were unbiased in terms of coupling state, precipitation, and temperature, which is a substantial improvement to the highly biased predictions from the CFSv2 forecasts. Furthermore, it was shown that the CSM based on local persistence provided some skill during the hindcast period when using observed initial conditions (CSMr); however, the statistical model based on correcting the coupling from the CFSRR (CCM) provided much better predictions of coupling state, precipitation, and temperature variables that were still unbiased. In this way the CCM is a bridging model (Hawthorne et al. 2013), as it uses forecasts of coupling state from a GCM to statistically generate precipitation and temperature predictions, but it is unique as it uses coupling state instead of climate indices like most bridging models. Although the SWM used in this study is unbiased and is skillful for seasonal forecasts, it lacks spatial coherence and only represents the precipitation and temperature at a point. This approach is reasonable for seasonal outlook forecasts of precipitation but can be problematic for use in forcing land surface models, as it does not account for the spatial correlations of the forecast variables. This could be improved by using a more complex model of precipitation and temperature that accounts for the spatial correlation. However, this would also increase the number of estimated parameters, which is already high at 120 per grid cell. Furthermore, the CSM (60) and CCM (20) also require a large amount of estimated parameters. Because of the large number of parameters, this framework

requires a large dataset in order to provide good estimates of the parameters. Furthermore, a distinct training and forecast period would be preferred, but this is not feasible with the limited temporal extent of the hindcast datasets; therefore, using a cross-validation framework by removing a single year from the training period provides the best approach for estimating the parameters. For a real-time application forecast, the hindcast dataset would serve as the training period and the model could be used to make real-time forecasts. In addition, there is also the possibility of reducing the number of parameters in the statistical models where there is little variability, such as removing the dependency of precipitation in the CSM for the atmospherically controlled regime (Fig. 2). Similar reductions could be done for the SWM that would reduce the number of parameters needed for utilizing this framework and make it more robust to smaller datasets.

Although there is potential for using statistical models based on coupling state for making real-time predictions as either stand-alone models or as bridging models, they were developed for attributing seasonal predictability. For instance, CSMr predictions of precipitation and temperature are solely based on the local persistence of initial conditions through a Markov chain model of coupling state and can be used to isolate the local coupling attribution. The CCM relies on the dynamical prediction of coupling state from CFSv2, but uses bias correction of the coupling and the SWM for precipitation and temperature. Therefore, the difference in the predictability of the CCM and the CSMr gives an estimate of the importance of a dynamical prediction of coupling state. Finally, the difference in the predictability of the CFSRR and the CCM gives an estimate of the attribution of predictability that is not associated with coupling (i.e., large-scale circulation and SST teleconnections) and is here denoted as noncoupling. The attribution of seasonal predictability due to local coupling was the lowest for precipitation and the highest for the daily maximum temperature, and, although the strength and extent varied, the intermountain region was the strongest for all three variables. In comparison, the attribution of dynamic coupling was more intense and covered a greater area, but was still mostly limited to west of the Mississippi. The attribution of noncoupling predictability was very weak for precipitation; however, it was much stronger in the southwestern and northern parts of the United States for daily maximum and minimum temperature. The attribution results indicate that the persistence of initial conditions through local coupling plays a role in seasonal prediction; however, it is greatly enhanced in the GCM, which considers the interactions in space and time and the influence of

TABLE A1. A list of crucial acronyms and terminology used in this study and their definitions.

Acronyms and terminology	Definition
CDI	Coupling drought index is a summary metric of the coupling state over a temporal period that was developed by Roundy et al. (2013). The CDI ranges from −1 (all wet coupling) to +1 (all dry coupling).
CCM	Coupling correction model provides predictions of the coupling state through the bias correction of the coupling state from CFSRR and is combined with the SWM to give predictions of precipitation and temperature.
CFSR	The Climate Forecast System Reanalysis assimilates observations with the CFSv2 model (Saha et al. 2010).
CFSR-LR	A subset of the CFSR data developed by Roundy et al. (2014) that is at a lower spatial resolution and utilizes fewer vertical levels in order to be consistent with the archived data of CFSRR.
CFSRR	The Climate Forecast System Reanalysis and Reforecast utilizes the CFSv2 model to create a 28-yr hindcast dataset of seasonal predictions of the coupled atmosphere–ocean–land climate system (Saha et al. 2014).
CFSv2	NCEP's Climate Forecast System, version 2, which is a global coupled atmosphere–ocean–land model (Saha et al. 2010, 2014).
Coupling state	A daily classification of land–atmosphere interactions into one of four states (wet coupling, dry coupling, transitional, or atmospherically controlled) based on soil moisture, atmospheric stability, and atmospheric humidity from Roundy et al. (2013).
CPM	Coupling potential model uses the observed coupling state from CFSR to make predictions of precipitation and temperature through the SWM.
CSM	Coupling stochastic model provides predictions of the coupling state based on a Markov chain model initialized by coupling state and precipitation.
CSMc	A version of CSM that is initialized with observed precipitation and climatological coupling state and is combined with SWM to give predictions of coupling state, precipitation, and temperature.
CSMr	A version of CSM that is initialized with observed precipitation and coupling state and is combined with SWM to give predictions of coupling state, precipitation, and temperature.
CTP	Convective triggering potential is a measure of atmospheric stability that is utilized in the classification of the coupling state.
HI	Humidity index is a measure of atmospheric humidity that is utilized in the classification of the coupling state.
SWM	Stochastic weather model provides predictions of precipitation, Tmax, and Tmin conditioned on coupling state.

other climate drivers. Furthermore, the results indicate that the intermountain region is a hotspot for seasonal prediction because of local persistence of initial conditions due to its high fraction of predictability for all variables. The extent to which these results are a representation of the strength of ''real world'' characteristics or simply an attribute of the CFSv2 modeling framework, from which the statistical models were derived, is unclear and requires further work.

The ability of the models to predict drought during JJA was also assessed. The results indicated that the persistence of the initial conditions through local coupling accounts for a portion of the drought area in 1988, but it completely missed the drought in the Midwest. Furthermore, the Midwest drought was captured in the predictions from the models that account for spatial interactions. This indicates that while the persistence of the initial conditions play a role in drought, the advective component is important for complete drought predictions. Furthermore, during the 1988 drought, the statistical models that were unbiased in their predictions of coupling provided better predictions of the precipitation during the drought than CFSRR; however, the daily maximum temperature predictions from the CFSRR were superior (Fig. 10). Considering 10 other

drought years during the hindcast period gave similar results in that the statistical models provided better predictions of precipitation during drought than the CFSRR, but the CFSRR provided better predictions of daily maximum temperature. This discrepancy is further complicated by the fact that, when considering the entire hindcast period, the CFSRR has a higher predictability for both precipitation and temperature (Fig. 7). One explanation is that the wet bias in the coupling state in CFSRR limits the representation of drought characteristics (Roundy et al. 2104). However, this would argue that both precipitation and daily maximum temperature would be limited, as both are affected by land–atmosphere interactions. The different response of the coupling state bias on the predictability of drought through precipitation and temperature could be due to the difference in the attribution of predictability seen in Fig. 9. For instance, the noncoupling portion of predictability is much stronger and covers a greater extent for daily maximum temperature compared to precipitation. This indicates that there is a much larger portion of the predictability of daily maximum temperature that would be unaffected by a bias in the coupling state. In addition, the difference could also be due to the fact that the statistical model for daily maximum temperature did not have as good of a fit as the statistical

model for precipitation (Fig. 3). It is likely that both of these reasons contribute to the discrepancy in the predictability of precipitation and daily maximum temperature in the models, but it is clear that the coupling bias does affect the prediction of drought from the CFSRR, as the statistical precipitation forecasts provide a better forecast as measured by the average threat score over the 11 drought years.

Although the predictability of drought for years like 1988 was good for all the models, there were years like 1983 when none of the models had any predictive skill for any of the variables. The inconsistency in the predictability across years and variables suggest that the mechanism of drought varies. For example, some years the drought is well described by the strong persistence of initial conditions and all models do fairly well. Other years the initial conditions play little role in the drought and the statistical models have no predictability, and the CFSRR is limited to only the noncoupling portion of predictability, which is much lower. This leaves a key question of what is driving this variability and how can this be identified in real time in order to provide confidence in the model predictions. More research is needed in order to understand this variability, but the framework presented here provides a means to better understand the relative importance of coupling state in seasonal forecasts with specific applications to drought prediction. Furthermore, it could be applied to similar modeling frameworks, like the NASA GEOS-5 (Rienecker et al. 2008, 2011), to understand the predictive variability across models. This could lead to further insights to the sensitivity of model parameters and drought predictability, which could lead to a better understanding of drought mechanism that could improve the practicality of drought forecasts.

APPENDIX

Acronyms and Terminology

Table A1 provides a list of acronyms and terminology used in this study.

REFERENCES

Dirmeyer, P. A., 2013: Characteristics of the water cycle and land–atmosphere interactions from a comprehensive reforecast and reanalysis data set: CFSv2. *Climate Dyn.,* **41,** 1083–1097, doi:10.1007/s00382-013-1866-x.

——, R. D. Koster, and Z. Guo, 2006: Do global models properly represent the feedback between land and atmosphere? *J. Hydrometeor.,* **7,** 1177–1198, doi:10.1175/JHM532.1.

Ek, M. B., K. E. Mitchell, Y. Lin, E. Rogers, P. Grunmann, V. Koren, G. Gayno, and J. D. Tarpley, 2003: Implementation of Noah land surface model advances in the National Centers for Environmental Prediction operational mesoscale Eta model. *J. Geophys. Res.,* **108,** 8851, doi:10.1029/2002JD003296.

Ferguson, C. R., and E. F. Wood, 2011: Observed land–atmosphere coupling from satellite remote sensing and reanalysis. *J. Hydrometeor.,* **12,** 1221–1254, doi:10.1175/2011JHM1380.1.

Findell, K. L., and E. A. B. Eltahir, 2003: Atmospheric controls on soil moisture–boundary layer interactions. Part I: Framework development. *J. Hydrometeor.,* **4,** 552–569, doi:10.1175/1525-7541(2003)004<0552:ACOSML>2.0.CO;2.

Goddard, L., S. J. Mason, S. E. Zebiak, C. F. Ropelewski, R. Basher, and M. A. Cane, 2001: Current approaches to seasonal to interannual climate predictions. *Int. J. Climatol.,* **21,** 1111–1152, doi:10.1002/joc.636.

Guo, Z., and Coauthors, 2006: GLACE: The Global Land–Atmosphere Coupling Experiment. Part II: Analysis. *J. Hydrometeor.,* **7,** 611–625, doi:10.1175/JHM511.1.

Hawthorne, S., Q. J. Wang, A. Schepen, and D. Robertson, 2013: Effective use of general circulation model outputs for forecasting monthly rainfalls to long lead times. *Water Resour. Res.,* **49,** 5427–5436, doi:10.1002/wrcr.20453.

Karl, T. R., and Coauthors, 2012: U.S. temperature and drought: Recent anomalies and trends. *Eos, Trans. Amer. Geophys. Union,* **93,** 473–474, doi:10.1029/2012EO470001.

Katz, R. W., 1977: Precipitation as a chain-dependent process. *J. Appl. Meteor.,* **16,** 671–676, doi:10.1175/1520-0450(1977)016<0671:PAACDP>2.0.CO;2.

Koster, R. D., M. J. Suarez, and M. Heiser, 2000: Variance and predictability of precipitation at seasonal-to-interannual timescales. *J. Hydrometeor.,* **1,** 26–46, doi:10.1175/1525-7541(2000)001<0026:VAPOPA>2.0.CO;2.

——, and Coauthors, 2006: GLACE: The Global Land–Atmosphere Coupling Experiment. Part I: Overview. *J. Hydrometeor.,* **7,** 590–610, doi:10.1175/JHM510.1.

——, Z. Guo, R. Yang, P. A. Dirmeyer, K. Mitchell, and M. J. Puma, 2009: On the nature of soil moisture in land surface models. *J. Climate,* **22,** 4322–4335, doi:10.1175/2009JCLI2832.1.

——, and Coauthors, 2011: The second phase of the Global Land–Atmosphere Coupling Experiment: Soil moisture contributions to subseasonal forecast skill. *J. Hydrometeor.,* **12,** 805–822, doi:10.1175/2011JHM1365.1.

Palmer, T. N., and D. L. T. Anderson, 1994: The prospects for seasonal forecasting—A review paper. *Quart. J. Roy. Meteor. Soc.,* **120,** 755–793, doi:10.1002/qj.49712051802.

Rienecker, M. M., and Coauthors, 2008: The GEOS-5 Data Assimilation System—Documentation of versions 5.0.1, 5.1.0, and 5.2.0. NASA/TM-2008-104606, Vol. 27, 101 pp. [Available online at http://gmao.gsfc.nasa.gov/pubs/docs/Rienecker369.pdf.]

——, and Coauthors, 2011: MERRA: NASA's Modern-Era Retrospective Analysis for Research and Applications. *J. Climate,* **24,** 3624–3648, doi:10.1175/JCLI-D-11-00015.1.

Roundy, J. K., C. R. Ferguson, and E. F. Wood, 2013: Temporal variability of land–atmosphere coupling and its implications for drought over the southeast United States. *J. Hydrometeor.,* **14,** 622–635, doi:10.1175/JHM-D-12-090.1.

——, ——, and ——, 2014: Impact of land–atmospheric coupling in CFSv2 on drought prediction. *Climate Dyn.,* **43,** 421–434, doi:10.1007/s00382-013-1982-7.

Saha, S., and Coauthors, 2010: The NCEP Climate Forecast System Reanalysis. *Bull. Amer. Meteor. Soc.,* **91,** 1015–1057, doi:10.1175/2010BAMS3001.1.

——, and Coauthors, 2014: The NCEP Climate Forecast System Version 2. *J. Climate,* **27,** 2185–2208, doi:10.1175/JCLI-D-12-00823.1.

Santanello, J. A., C. D. Peters-Lidard, S. V. Kumar, C. Alonge, and W.-K. Tao, 2009: A modeling and observational framework for diagnosing local land–atmosphere coupling on diurnal time scales. *J. Hydrometeor.,* **10,** 577–599, doi:10.1175/2009JHM1066.1.

——, ——, and ——, 2011: Diagnosing the sensitivity of local land–atmosphere coupling via the soil moisture–boundary layer interaction. *J. Hydrometeor.,* **12,** 766–786, doi:10.1175/JHM-D-10-05014.1.

Taylor, C. M., R. A. M. de Jeu, F. Guichard, P. P. Harris, and W. A. Dorigo, 2012: Afternoon rain more likely over drier soils. *Nature,* **489,** 423–426, doi:10.1038/nature11377.

Wilhite, D. A., 2000: Drought as a natural hazard: Concepts and definitions. *Drought: A Global Assessment.* Routledge, 3–18.

Xia, Y., and Coauthors, 2012: Continental-scale water and energy flux analysis and validation for the North American Land Data Assimilation System project phase 2 (NLDAS-2): 1. Intercomparison and application of model products. *J. Geophys. Res.,* **117,** D03109, doi:10.1029/2011JD016048.